Attenuation of Self-Excited Roll Oscillations of Low-Aspect-Ratio Wings by means of Acoustic Forcing

T. Hu[1], Z. Wang[2] and I. Gursul[3]

University of Bath, Bath, BA2 7AY, United Kingdom

Abstract

Attenuation of self-excited roll oscillations of low-aspect-ratio wings using acoustic excitation was studied in a wind tunnel. For a rectangular flat plate wing with an aspect ratio of 2, roll oscillations can be completely suppressed and the onset of the roll oscillations can be delayed with external acoustic excitation. Similar results were also obtained for wings with two different airfoil profiles. Velocity measurements indicated that acoustic excitation could restore a symmetric vortex flow over the free-to-roll wings thus eliminating the self-excited roll oscillations. The effect of excitation is most noticeable for the side of the wing that sees a larger effective angle of attack due to the rolling motion. Acoustic excitation energizes the shear layer instabilities and results in reattachment or smaller separated flow region closer to wing surface, thus in turn suppressing the roll oscillations.

[1] Postgraduate Student, Department of Mechanical Engineering.
[2] Lecturer, Department of Mechanical Engineering, Member AIAA.
[3] Professor, Department of Mechanical Engineering, Associate Fellow AIAA.

Nomenclature

b = wing span

c = wing chord

f = frequency

I_{xx} = moment of inertia about x-axis

Re = Reynolds number, $\rho U_\infty c/\mu$

St = Strouhal number, fc/U_∞

t = maximum thickness of wing

U = velocity in a streamwise plane

U_∞ = freestream velocity

x = chordwise coordinate

y = spanwise coordinate

z = distance normal to the freestream

α = wing angle of attack

μ = viscosity

ρ = density

ω = vorticity

Φ = roll angle

Λ = wing sweep angle

AR = aspect ratio

FFT = fast Fourier transform

LAR = low aspect ratio

MAV = micro air vehicle

PIV = particle image velocimetry

SPL = sound pressure level

UAV = unmanned air vehicle

rms = root-mean-square

$|Y(f)|$ = power spectrum density of velocity fluctuations

I. Introduction

Research and development of unmanned air vehicles (UAVs) and micro air vehicles (MAVs) has been receiving increasing interest because of their broad range of applications. MAVs have operating speeds around 10 m/s with a maximum dimension between 10 and 15 cm. For fixed-wing MAV applications, aerodynamics of low-aspect-ratio (LAR) wings in various airfoil and planform shapes at low Reynolds numbers have been investigated recently [1,2].

Roll instabilities and oscillations are inherent to fixed-wing MAVs due to their low aspect ratio wings and low mass moment of inertia [3]. Self-induced limit-cycle roll oscillation of *slender* delta wings, referred to as "wing-rock", is a well-known fluid-structure interaction, and is driven by the leading-edge vortices [4,5]. The majority of previous studies on the aerodynamics of free-to-roll low aspect ratio wings was limited to slender delta wings and rectangular wings with aspect ratio *AR* below 0.5 [6,7]. Recent studies on free-to-roll non-slender delta wings showed that self-induced roll oscillations also exist for delta wings with sweep angles $\Lambda \leq 60^{o}$, but with a nonzero mean roll angle when the wing is around the stall angle [8-10]. For these low sweep angle wings, nonzero trim angles are observed until the wing stalls after which the trim angle becomes zero. In a certain range of sweep angles and just before the stall, large amplitude self-induced roll oscillations with nonzero mean are observed. More recently, experimental investigations on relatively higher aspect ratio (*AR* = 2 and 4) rectangular flat plate wings suggested that, even at pre-stall incidences, self-excited roll oscillations occur [11,12]. These results showed that the self-induced roll motion is

driven by a time lag in the strength of the tip vortices. Velocity measurements also showed that the onset of the roll oscillations is related to the loss of reattachment of the leading-edge separation bubble. Roll oscillations with very large amplitude have been observed in the flight tests of various MAVs [13] and are difficult to control. As the roll oscillations appear at moderate to high angle of attack [11,12], this situation is unavoidable in a gust that causes the effective angle of attack to increase. Consequently, obtaining stable video footage may become very difficult in atmospheric disturbances.

The present research is focussed on the suppression of the self-induced roll oscillations of a rectangular wing with aspect ratio of 2, using acoustic excitation. Previous studies on attenuation of slender wing rock have been conducted by applying both passive [14] and active flow control techniques (such as flaps and blowing) [15-18]. Katz [5] reviewed these methods and concluded that the active techniques tend to be more effective for slender delta wings. In the present study, we show that acoustic excitation can eliminate the roll oscillations of a low aspect ratio rectangular wing. Initial experiments have been presented at a conference [19]. In the present manuscript, we extend these previous experiments so as to explain the flow physics. Acoustic excitation has been previously studied in order to delay the boundary layer separation as well as to enhance the shear layer reattachment over an airfoil [20-25]. Active flow control can often be regarded as periodic addition of momentum that affects the boundary layers and shear layers [26]. As separated flows are dominant over the leading-edge and tips of a low aspect ratio wing, active flow control with acoustic excitation offers the potential to increase the robustness of MAVs to atmospheric disturbances. This paper presents an experimental study and investigates the mechanism of the attenuation of roll oscillations. Acoustic excitation allows us to vary the excitation frequency in a wide range while keeping the forcing amplitude constant.

II. Experimental Apparatus and Methods

A. Closed-loop wind tunnel

The experiments were conducted in a closed-loop wind tunnel located at the Department of Mechanical Engineering of the University of Bath. The test section of the wind tunnel has dimensions of 2.13 × 1.52 × 2.70 m. The tunnel has a turbulence level of less than 0.1%. Figure 1 shows the experimental arrangement including the layout of the working section, the acoustic excitation system located at the side wall of the test section and the high-alpha rig. The high-alpha rig allows the angle of attack to be varied as the wind tunnel is running with an accuracy of ±0.25 degrees. Note that the high-alpha rig shown in Figure 1, upon which the wing model was mounted, is independent of the wind tunnel structure. Therefore, any possible structural vibrations of the wind tunnel caused by the speaker are not transmitted through the support to the wing model.

B. Free-to-roll (FTR) device

The free-to-roll device consists of a shaft that is supported in greased bearings, so is free to rotate with minimal friction. One end of the shaft is attached to a potentiometer which outputs a varying voltage, linearly dependent on the roll angle, while the other end of the shaft is attached to the sting upon which the wing is supported (Figure 1). The output from the potentiometer was fed to the computer via an A-D converter at a sampling frequency of 200 Hz for 120 seconds over a range of angles of attack with an estimated uncertainty of $\pm 1^{o}$. From these data, the amplitude of the roll angle of the oscillations was calculated, as well as the maximum and minimum roll angles achieved during the recorded time period. The stings used for all the models on the free-to-roll device were in line with the roll axis of the wings themselves as shown in Figure 2, so there was no coning motion, just pure roll.

C. Models

Three rectangular wings, of flat plate, NACA0012 and SD7003-085-88 profiles, with an aspect ratio of AR = 2 were tested. The sting used for all the wings was attached to the pressure surface of the model, resulting in a suction surface with no protrusions, as shown in Figure 2. All the wings have a chord length of 167.5 mm, similar mass (within 2% difference) and moment of inertia (within 2.5% difference) about the roll-axis. The physical properties of the wings are shown in Table 1. The flat plate was made out of 3 mm aluminium plate with round edges (semi-circular shape). The NACA0012 and SD7003-085-88 wings were hollow structures manufactured by SLS rapid prototyping. The tips (side-edge) of the NACA0012 and SD7003-085-88 wings were rounded with a semi-circle profile (Figure 2). Experiments were conducted at a free stream velocity of U_∞ = 10 m/s (Re = 1.14×10^5 based on wing root chord length) for all three wings. The maximum blockage was approximately 2.3%. The models were painted matt black in order to reduce reflections created from the laser sheet during the PIV tests, which will be discussed in detail in Section II-E. The moment of inertia about the roll axis for each wing was calculated using CAD software, which was calibrated using the measured masses of the wings, and includes the moment of inertia of the sting used.

D. Acoustic excitation

The acoustic excitation was provided by an 800-Watts Eminence Omega PRO-18A speaker with a working frequency range of f = 35 to 120 Hz (St = 0.6 – 2 based on wing root chord length) driven by a high power performance Soundmaster VF400 amplifier. The speaker has a diameter of 457 mm and is about 1 meter away from the wing model. The speaker was mounted on a wood board attached to the side frame of the test section and aligned with the wing facing the suction surface (see Figure 1). We have not varied the

location of the speaker in the experiments. However, given the large dimensions of the speaker with respect to the wing as well as large acoustic wavelength, we expect relatively uniform sound pressure level (SPL) over the wing surface. The sound pressure level (SPL) of the acoustic excitation, measured at the mid-span of the leading-edge of the wing in absence of the freestream flow, was calibrated using probe-type microphones and a precision acoustic calibrator. The effective SPL was kept constant at 110 dB for all acoustic excitation frequencies tested. The sound pressure level was varied in the preliminary experiments. Higher sound pressure levels could not be achieved due to the power limitation of the speaker. SPL=110 dB was chosen because it resulted in effective control of the roll oscillations while allowing to keep the SPL constant (by varying the input voltage) for a wide range of excitation frequencies of the speaker.

Table 1. Properties of wings tested

Wing	Flat plate	NACA0012	SD7003-085-88
Airfoil profile			
Chord length, c	167.5 mm	167.5 mm	167.5 mm
Aspect ratio, AR	2	2	2
Maximum thickness t	3 mm	20.1 mm	14.3 mm
Leading-edge profile	round (semicircle)	--	--
Side-edge profile	round (semicircle)	round (semicircle)	round (semicircle)
Material	aluminium	polyamide with aluminium reinforcement	polyamide with aluminium reinforcement
Mass	0.443 kg	0.436 kg	0.441 kg
Moment of inertia, I_{xx}	0.0040 kgm^2	0.0039 kgm^2	0.0040kg m^2

E. Particle image velocimetry (PIV) system

Quantitative flow measurements were undertaken using two different Particle Image Velocimetry (PIV) systems. The first system, a TSI 2D-PIV system consisting of dual 50 mJ Nd:YAG lasers and an 8-bit CCD camera with a resolution of 1600 by 1192 pixels, was used to measure time-averaged and phase-averaged velocity fields for the $AR = 2$ flat plate wing. Measurements were taken in a crossflow plane near the trailing edge of the wing, and also in streamwise planes at various spanwise locations. The flow was seeded with oil droplets produced by a TSI model 9307-6 multi-jet atomizer. The atomizer worked best using olive oil and the mean size of the droplets was 1 μm. The maximum repetition rate of the PIV system was 7.25 Hz in the cross-correlation mode. PIV measurements were conducted for both the stationary wing and the free-to-roll wing, with dynamic roll angle (Φ) increasing and decreasing. For experiments with stationary wings, tests were performed while the wing was clamped at the desired roll angle. For the free-to-roll measurements, phase-averaged velocity measurements were performed by triggering the laser at specific roll angles during the roll oscillations. An error of ±0.5° in the trigger angle existed in these measurements. Three separate tests in the cross-flow plane were needed to cover the whole extent of the wing span. The PIV images were analysed using the software Insight 3G with a fast Fourier transform (FFT) cross-correlation algorithm and a Gaussian peak engine to obtain the velocity vectors. The recursive interrogation window size was 48 by 48 pixels for the crossflow measurements and 32 by 32 pixels for measurements in streamwise planes. The effective grid size varied from 2.3 mm to 3.1 mm in these measurements. Sequences of 500 images were taken in each measurement.

In order to study the spectral features of the shear layer separated from the leading edge of the wings tested, the second system, a TSI high frame-rate PIV system, was used to measure the flow fields in the streamwise planes. Illumination of the desired plane was

achieved using a New Wave Pegasus Nd:YLF double pulse high speed laser with a maximum energy of 10 mJ per pulse. The laser light sheet was placed parallel to the freestream velocity. The images were captured using a TSI PowerView HS-3000 high speed CMOS camera with the resolution of 1024×1024 pixels. A TSI LaserPulse synchroniser unit was utilized to link the camera and the laser to enable the accurate capture for two frame cross-correlation analysis. Seeding was provided by the same atomizer used with the first system. The images were analyzed with the Insight 3G software using the same FFT cross-correlation algorithm and a Gussian peak engine to obtain the velocity vectors. The interrogation window size was 16 by 16 pixels and the effective grid size varied from 0.9 mm to 1 mm. The system was operated at 2 kHz. This allowed the capture of velocity field at 1 kHz and 6000 instantaneous images were captured for each of the measurement planes. The measurement uncertainty for the velocity was estimated as 2% of the free stream velocity.

III. Results and Discussion

A. Free-to-roll flat plate wing

Figure 3 presents the variations of mean, minimum and maximum roll angle with angle of attack of the flat plate wing without and with acoustic excitation at St = 1.5. When there was no acoustic excitation, prior to $\alpha = 11^{o}$, nonzero mean roll angles were observed. It was shown by Gresham *et al.* [12] that asymmetric leading-edge bubbles and therefore asymmetric tip vortices were possible at low incidences, resulting in nonzero mean roll angles. When the wing incidence was increased to $\alpha = 12^{o}$, small amplitude roll oscillations occurred, and the roll amplitude increased gradually with increasing angle of attack until $\alpha = 15^{o}$. A sharp increase in the amplitude of the wing roll oscillations can be observed at about $\alpha = 15^{o}$. For $\alpha \geq 17°$, the amplitude of the wing roll oscillations increased gradually and eventually saturated. Note that for $\alpha \geq 12^{o}$, the mean roll angle remains close to zero degrees.

When acoustic excitation was applied at St = 1.5, the onset of the self-excited roll oscillations was delayed by approximately 4° of wing incidence to about α = 16° (Figure 3). A sharp increase in the amplitude of the wing roll oscillations was observed at about α = 18.5°. At about α = 20°, the amplitude of the wing roll oscillations approached the same values as that of the experiments without acoustic excitation. Note that Figure 3 indicated that the acoustic excitation had little effect on the mean roll angle, which remained near zero for α ≥ 12°. The time histories of the wing roll angle with and without acoustic control at α = 17° are presented in Figure 4. It can be observed that, when there was no acoustic control, the roll oscillations exhibit periodic nature with amplitude of about 40°. The corresponding Strouhal number of these oscillations is very low: $St \approx 0.0089$. The acoustic excitation at St = 1.5 results in a significant reduction of the roll amplitude to a few degrees.

The effectiveness of the acoustic excitation frequency in reducing and delaying roll oscillations on the flat plate wing is presented in Figures 5 and 6. Figure 5 suggests that, for St = 0.75, the acoustic excitation has little or no effect on the RMS values of the roll angle for all angles of attack tested. For $1.1 \leq St \leq 1.5$, the effectiveness of roll suppression increases with increasing Strouhal number. With further increasing Strouhal number (St >1.5), the effectiveness of acoustic excitation decreased. Note that, for all St tested, acoustic excitation has little or no effect on the amplitude of roll oscillations at α < 15° or α > 19°. Figure 6 shows the RMS values of the roll angle as a function of Strouhal number of the acoustic excitation for 15° ≤ α ≤ 19°, within which the acoustic excitation effectiveness was significant. For all the values of α tested, a local minimum in RMS value of the roll angle is observed at around St = 1.5. Therefore, the optimum acoustic excitation frequency for attenuation of the roll oscillations corresponds to St = 1.5 for the flat plate wing. Figures 5 and 6 also show that, at the optimum excitation frequency of St = 1.5, the maximum values of RMS roll angle suppression, $\Delta\Phi_{rms,max}$, of about 30° was achieved at α = 17°. Furthermore, as

discussed earlier, the maximum delay by approximately $\Delta\alpha_{max} = 4°$ in the onset of the self-excited roll oscillations was achieved at $St = 1.5$ (Figures 3 and 5).

B. Other wings

The variations of mean, minimum and maximum roll angle with angle of attack of the NACA0012 wing and SD7003-085-88 wing exhibit similar trends to those of the flat plate wing. Figure 7a indicates that, when there was no acoustic excitation applied on the NACA0012 wing, nonzero mean roll angles were observed at low incidences up to $\alpha = 13°$. Small amplitude roll oscillations occurred at around $\alpha = 14°$. For $\alpha > 14°$, the amplitude of the self-excited wing roll oscillation increased gradually with increasing angle of attack. The acoustic excitation at $St = 1.5$ delayed the onset of self-excited roll oscillations by about 3° to $\alpha = 17°$. Following a sharp increase at around $\alpha = 18.5°$, the amplitude of the NACA0012 wing roll oscillations approached the same values as that of the experiments without acoustic excitation at about $\alpha = 20°$. Similar results were also observed for the SD7003-085-88 wing (Figure 7b). For example, when there was no acoustic excitation, a nonzero mean roll angle was observed for $\alpha < 14°$. Roll oscillations started at $\alpha = 14°$ and its amplitude increased with angle of attack. Acoustic excitation at $St = 1.45$ delayed the onset of roll oscillation by 3° to $\alpha = 17°$. At about $\alpha = 21°$, the oscillation approached the same amplitude as in the no acoustic excitation scenario.

The effects of the acoustic excitation frequency on the self-excited roll oscillations of the NACA0012 wing and SD7003-085-88 wing are presented in Figures 8 and 9, which again exhibit similar trends to the flat-plate wing case (Figures 5 and 6). For example, the most effective suppression for the NACA0012 wing was observed at around $St = 1.5$. For $\alpha = 17°$ and $St = 1.5$, the acoustic excitation reduced the RMS value of the wing roll angle by approximately 16° and delayed the onset of the roll oscillation by $\Delta\alpha_{max} \approx 2.6°$ (Figures 7a

and 8a). For the SD7003-085-88 wing according to Figures 7b and 8b, the optimum excitation frequency was observed at St = 1.45, which is close to that of the flat plate wing and NACA0012 wing cases. It was found that at $\alpha = 17°$ and St = 1.45, the acoustic excitation reduced the RMS value of wing roll oscillation by approximately 18° and delayed the onset of roll oscillation by $\Delta\alpha_{max} \approx 3°$.

C. Velocity measurements for the flat plate wing

The aforementioned results suggest that for all three wings tested, regardless of the airfoil profiles, the most effective acoustic excitation frequencies in suppressing the self-excited roll oscillations were within the range St = 1.45-1.5. Flow measurements are needed to understand the physics behind these observations. Previous studies have indicated that the characteristics of tip vortices and leading-edge separation play an important role in the onset and magnitude of the self-excited roll oscillations [12]. Therefore, PIV measurements were conducted on both stationary and free-to-roll flat plate wing without and with acoustic excitation of St = 1.5 for $\alpha = 17^o$ and a roll angle of $\Phi = 0^o$. Figure 10 presents the time-averaged and phase-averaged velocity magnitude and streamline patterns over the flat plate wing at spanwise locations of y/(b/2) = 0 (mid-span), ±0.5, ±0.75, and ±0.97, where the minus sign represents the left half of the wing and the plus sign represents the right half of the wing, as viewed from downstream. For the stationary wing, the flow was fully separated at the mid-span (y/(b/2) = 0), but mostly attached at the wing tip (y/(b/2) = ±0.97) (Figure 10a), due to the effects of the tip vortices [12]. The acoustic excitation had some effect on the flow structure over the stationary wing, i.e., the center of the recirculation region seen in the time-averaged streamline pattern moved slightly towards the leading-edge at mid-span location (y/(b/2) = 0) and quarter span locations (y/(b/2) = ±0.50) (Figure 10b).

In the absence of acoustic forcing, an asymmetric flow structure was observed over the free-to-roll wing. When $\Phi = 0^o$ and increasing (wing rotating in the counter-clockwise direction) as shown in Figure 10c, the phase-averaged flow separation region appears to be larger in the left half of the wing (most noticeable at y/(b/2) = –0.50). Similarly, when Φ is decreasing (wing rotating in the clockwise direction), the right half of the wing reveals larger separation (Figure 10e). Note that this type of asymmetric flow structure is typical of self-induced roll oscillations [11,12]. Figures 10d and 10f suggest that, when acoustic excitation at St = 1.5 is applied the flow structure becomes more symmetric, which attenuates the self-excited roll oscillations. Note that acoustic excitation had a smaller effect on the phase-averaged flow structure at the mid-span.

Figure 11 presents the phase-averaged velocity magnitude, velocity standard deviation and vorticity over the free-to-roll flat plate wing at $\Phi = 0°$ (increasing), for y/(b/2) = –0.5. These are the conditions where the most significant acoustic excitation effect was observed (Figures 10c and d). It can be seen from Figure 11 that, when acoustic excitation is applied, the separated flow moves closer to the wing surface, the recirculation region becomes smaller and it moves upstream. Effectively, acoustic excitation generates a local flow field that is more characteristic of a lower incidence. The vorticity contours suggest that, when the acoustic excitation is applied, the leading edge shear layer separates at a smaller angle (Figures 11e and f), which is consistent with the above observations. It is interesting to note that, for the free-to-roll wing, acoustic excitation has a larger effect on the flow structure at y/(b/2) = –0.5 than y/(b/2) = 0 (mid-span) (Figure 10).

Figure 12 presents the vorticity patterns in the crossflow plane near the trailing edge of the flat plate wing for $\alpha = 17°$ and $\Phi = 0°$. It can be observed that the vorticity pattern was fairly symmetric over the stationary wing (Figure 12a). For the free-to-roll wing, when the wing was rolling clockwise (Φ decreasing), an asymmetric vorticity pattern was observed,

i.e., a compact vortex near the left-hand-side wing tip and a weaker (less coherent) vortical structure further away from the wing surface near the other wing tip (Figure 12b). Note that the hysteresis and time lag effects, resulting in the asymmetric vortex flows, have been reported previously [11,12]. Figure 12c suggests that the acoustic excitation restored the vorticity field back to a symmetric pattern, which was similar to the stationary case. It is apparent in Figure 12 that the effect of acoustic excitation is more significant on the tip vortex on the right-hand side. In the absence of excitation, this vortex is located further away from the wing and sees a larger "effective" angle of attack due to the rolling motion (Figure 12b). Also, Figure 12 suggests that the mechanism of the suppression of the roll oscillations may be related to the movement of this tip vortex closer to the wing. In a way, the tip vortex and local separated flow become similar to what is expected for a smaller angle of attack. The tip vortex on the other (left-hand) side is little affected by excitation. It should be kept in mind that the tip vortex is part of the three-dimensional separation region. Figure 13 shows the standard deviation of the velocity fluctuations in the crossflow plane near the trailing edge of the flat plate wing. The asymmetric separation region for the rolling wing (Figure 13b) becomes more symmetric with acoustic forcing (Figure 13c). The excited flow field appears similar to the unexcited flow for the stationary wing (Figure 13a). Tip vortices form further away from the wing in the static case at high angle of attack. Vortex-wing interaction and the hysteresis in the location of the tip vortices lead to the onset of the self-excited roll oscillations. With acoustic forcing, the separated shear layer becomes closer to the wing surface, resulting in the formation of the tip vortices closer to the surface as well. This is equivalent to the flow conditions at a smaller angle of attack, and prevents the onset of the self-excited roll oscillations. In the following section, we investigated the spectral features of the separated shear layer in streamwise planes.

D. Spectral features of separated flow

Acoustic forcing is a global flow control approach, thus both tip vortex and shear layer separated from the leading-edge are excited at the same time. In order to understand the effects better, high-frame-rate PIV measurements were conducted to study the unsteadiness of the separated shear layer from the leading edge. Figures 14 and 15 show the time-averaged velocity magnitude and streamline patterns over the stationary flat plate wing near the leading edge and in the streamwise plane at y/(b/2) = 0 (mid-span) and y/(b/2) = 0.5 (quarter-span) for $\alpha = 17°$ without and with acoustic forcing at various frequencies. For each case, frequency spectra of streamwise velocity fluctuations are calculated from the PIV data near the shear layer at the location $x/c = 0.25$, which are denoted by symbol '+' in Figures 14 and 15. The velocity magnitude and streamline patterns indicate separated flows at the mid-span and quarter-span. At y/(b/2) = 0, the frequency spectra of the no acoustic forcing case exhibits a dominant peak at around $fc/U_\infty \approx 1.5$ (Figure 14a). It is believed that this peak corresponds to the dominant frequency of the natural shear-layer instabilities. This dominant frequency of shear layer instabilities is however not identified by the current PIV measurements at y/(b/2) = 0.5 (Figure 15a), possibly due to the three-dimensional nature of the separated shear layer and the effect of the tip vortices.

With acoustic forcing at $St = 0.6$, no dominant peak is observed in the velocity spectrum at y/(b/2) = 0 (Figure 14b) and y/(b/2) = 0.5 (Figure 15b), because this frequency is not close to the natural frequency of the shear layer. When the frequency of acoustic excitation is increased to $St = 1.5$, both velocity spectra at the mid-span (Figure 14c) and quarter-span (Figure 15c) exhibit a sharp dominant peak at the same frequency as the acoustic excitation, suggesting strong resonance between the acoustic forcing and shear layer instabilities. With further increase in the frequency of acoustic excitation to $St = 2.0$, the velocity spectrum at y(b/2) = 0 (Figure 14d) and y(b/2) = 0.5 (Figure 15d) exhibit prominent

peaks at the forcing frequency but with much smaller amplitude than those observed in the *St* = 1.5 case, suggesting a weakening resonance. Previous studies indicate that large amplitude self-excited roll oscillations occur when the flow is fully separated from the low aspect ratio rectangular wing surface [12]. Therefore, the strong resonance observed at *St* = 1.5 energizes the shear layer separated from the leading edge and results in local reattachment (Figure 11b) or smaller separated region closer to the wing surface, which attenuates the roll oscillations. Although this method may be used by emitting sound waves from the fuselage of the fixed-wing MAVs, local excitation of the separated flow may be more effective in practical applications.

The time-averaged streamline patterns, together with the frequency spectra of streamwise velocity fluctuations calculated near the shear layer at x/c = 0.25, y/(b/2) = 0 (mid-span) and $\alpha = 17°$ over the stationary NACA0012 wing and SD7003-085-88 wing are presented in Figures 16 and 17, respectively. In general, Figures 16 and 17 exhibit similar features as the results for the flat plate wing. For example, the velocity spectrum exhibits major peaks at *St* = 1.5 for the NACA0012 wing (Figure 16c) and *St* = 1.45 for the SD7003-085-88 wing (Figure 17c), suggesting strong resonance between the shear layer instabilities and the acoustic forcing, which becomes weaker with further increase in excitation frequency (Figure 16d & 17d). Note that the amplitudes of the peaks in Figures 16c & 17c are smaller than its counterpart for the flat plate wing (Figure 14c). The reasons are not known, however may be due to the fact that the flow separation point is not fixed for round leading-edges. Again, no dominant peak is observed in the velocity spectrum for excitation at *St* = 0.6 (Figures 16b & 17b). The present results suggest that all three wings tested share the same mechanism of effective control of self-excited roll oscillations using acoustic excitation. The separated shear layer is excited and this promotes local reattachment or a smaller separated flow region which is closer to the wing surface. Effectively, this is similar to the action of

lowering the angle of attack, and delays the onset of the large amplitude self-excited roll oscillations. Due to the similarity of the separated shear layer, the optimum Strouhal number is similar for all three wings.

IV. Conclusions

An experimental investigation of the attenuation of self-excited roll oscillations of low aspect ratio wings using acoustic excitation has been performed. Roll angle histories over a range of incidences were measured, and it was found that the roll oscillations first appeared at pre-stall incidences and increased with increasing angle of attack. When the acoustic excitation is applied, these roll oscillations can be effectively suppressed. For a flat plate wing, at the optimum acoustic excitation frequency of St = 1.5; the magnitude of roll oscillation can be suppressed up to $\Delta\Phi_{rms,max} \approx 30°$ and the onset of the roll oscillations can be delayed up to $\Delta\alpha_{max} \approx 4°$. Similar results were obtained for the NACA0012 wing and the SD7003-085-88 wing cases. For the NACA0012 wing, the optimum excitation frequency of St = 1.5 produces: $\Delta\Phi_{rms,max} \approx 16°$ and $\Delta\alpha_{max} \approx 2.6°$. For the SD7003-085-88 wing, the optimum excitation frequency of St = 1.45 produces: $\Delta\Phi_{rms,max} \approx 18°$ and $\Delta\alpha_{max} \approx 3°$.

Velocity measurements taken over the flat plate wing in a crossflow plane near the trailing edge and in various streamwise planes indicated that the acoustic excitation could return the asymmetric flows over the free-to-roll wing back to a symmetric pattern, which attenuates the self-excited roll oscillations. The effect of excitation is largest for the tip vortex which forms further away from the wing in the absence of excitation. This vortex moves closer to the wing with excitation, and the vorticity field becomes more symmetric. The effect of excitation is small at the mid-span, but may be significant at other spanwise stations depending on whether the roll angle is increasing or decreasing. Large effects of excitation

were observed on the side of the wing that sees a larger effective angle of attack due to the rolling motion. Hence both the tip vortex and the shear layer separated from the leading-edge are altered with excitation. The effect of the acoustic excitation is to produce a flow field that is more typical of a lower angle of attack.

Time-resolved high-frame-rate PIV measurements taken in various streamwise planes revealed strong resonance between acoustic forcing and instabilities of the shear layer separated from the leading edge when the acoustic excitation was applied at the optimum frequency. The excitation energizes the separated shear layer and results in local reattachment or a smaller separated flow region that is closer to the wing surface. This generates a flow field similar to that of a smaller incidence, and attenuates the self-excited wing roll oscillations. This mechanism of control of the roll oscillations using acoustic excitation is similar for all three wings tested regardless of airfoil profile.

Acknowledgments

This work was supported by the RCUK Academic Fellowship in Unmanned Air Vehicles. The authors would like to thank the EPSRC Engineering Instrument Pool, and also Dr. David Cleaver for reading the manuscript.

References

1. Pelletier, A. and Mueller, T. J., "Low Reynolds Number Aerodynamics of Low-Aspect-Ratio, Thin/Flat/Cambered-Plate Wings ", *Journal of Aircraft*, Vol. 37, No. 5, 2000, pp. 825 - 832.

2. Torres, G. E. and Mueller, T. J., "Low-Aspect-Ratio Wing Aerodynamics at Low Reynolds Numbers", *AIAA Journal*, Vol. 42, No. 5, 2004, pp. 865 - 873.

3. Mueller, T., *Fixed and Flapping Wing Aerodynamics for Micro Air Vehicle Applications*, Published by the AIAA, 2001.

4. Arena, A. S. J. and Nelson, R. C., "Experimental Investigation on Limit Cycle Wing Rock of Slender Wings", *Journal of Aircraft*, Vol. 31, No. 5, 1994, pp. 1148 - 1155.

5. Katz, J., "Wing/Vortex Interactions and Wing Rock", *Progress in Aerospace Sciences*, Vol. 35, 1999, pp. 727-750.

6. Levin, D. and Katz, J., "Self-Induced Roll Oscillations of Low-Aspect-Ratio Rectangular Wings," *Journal of Aircraft*, vol. 29, No. 4, 1992, pp. 698-702.

7. Williams, D. L. and Nelson, R. C., "Fluid-Dynamic Mechanisms Leading to the Self-Induced Oscillations of LARR Wings," AIAA 97-0830, *35th Aerospace Sciences Meeting & Exhibit*, 1997, Reno, NV.

8. Matsuno, T. and Nakamura, Y., "Self-Induced Roll Oscillation of 45-degree Delta Wings," AIAA 2000-0655, *38th AIAA Aerospace Sciences Meeting and Exhibit*, 10th-13th January 2000, Reno, NV.

9. Gursul, I., Gordnier, R. and Visbal, M., "Unsteady Aerodynamics of Nonslender Delta Wings", *Progress in Aerospace Sciences*, Vol. 41, 2005, pp. 515 - 557.

10. Gresham, N. T., Wang, Z. and Gursul, I., "Vortex Dynamics of Free-to-Roll Slender and Nonslender Delta Wings", *Journal of Aircraft*, Vol. 47, No. 1, 2010, pp. 292 - 302.

11. Gresham, N. T., Wang, Z. and Gursul, I., "Self-Induced Roll Oscillation of Non-slender Wings", *AIAA Journal*, Vol. 47, No. 3, 2009, pp. 481-483.

12. Gresham, N. T., Wang, Z. and Gursul, I., "Low Reynolds Number Aerodynamics of Free-to-Roll Low Aspect Ratio Wings", *Experiments in Fluids*, Vol. 49, 2010, pp. 11 - 25.

13. Krashanitsa, R., Platanitis, G., Silin, D. and Shkarayev, S., "Autopilot Integration into Micro Air Vehicles", in *Introduction to the Design of Fixed-Wing Micro Air Vehicles* edited by Mueller, Kellogg, Ifju, Shkarayev. Published by the AIAA, 2007.

14. Mabey, D. G., "Similitude Relations for Buffet and Wing Rock on Delta Wings ", *Progress in Aerospace Sciences*, Vol. 33, 1997, pp. 481 - 511.

15. Katz, J. and Walton, J., "Control of Wing Rock Using Leading-Edge Vortex Manipulations", AIAA 92-0279, *AIAA Aerospace SciencesMeeting*, 1992, Reno, NV.

16. Katz, J. and Walton, J., "Application of Leading-Edge Vortex Maniplations to Reduce Wing Rock Amplitudes", *Journal of Aircraft*, Vol. 30, No. 4, 1993, pp. 555 - 557.

17. Wong, G. S., Rock, S. M., Wood, N. J. and Roberts, L., "Active Control of Wing Rock Using Tangential Leading-Edge Blowing", *Journal of Aircraft*, Vol. 31, No. 3, 1994, pp. 659 - 665.

18. Sreenatha, A. G. and Ong, T. K., "Wing Rock Suppression Using Recessed Angle Spanwise Blowing ", *Journal of Aircraft*, Vol. 39, No. 5, 2002, pp. 900 - 903.

19. Hu, T., Wang, Z. and Gursul, I., "Control of Self-Excited Roll Oscillations of Low-Aspect-Ratio- Wings Using Acoustic Excitation", AIAA-2011-36, AIAA Conference, 4-7 January 2011, Orlando.

20. Nishioka, M., Asia, M. and Yoshida, S., "Control of Flow Separation by Acoustic Excitation", *AIAA Journal*, Vol. 28, No. 11, 1990, pp. 1909 - 1915.

21. Zaman, K. B. M. Q. and McKinzie, D. J., "Control of Laminar Separation over Airfoils by Acoustic Excitation", *AIAA Journal*, Vol. 29, No. 7, 1991, pp. 1075 - 1083.

22. Zaman, K. B. M. Q., "Effect of Acoustic Excitation on Stalled Flows over an Airfoil", *AIAA Journal*, Vol. 30, No. 6, 1992, pp. 1492 - 1499.

23. Hsiao, F.-B., Jih, J.-J. and Shyu, R.-N., "Effect of Acoustics on Flow Passing a High-AOA Airfoil ", *Journal of Sound and Vibration*, Vol. 199, No. 2, 1997, pp. 177 - 188.

24. Yarusevych, S., Kawall, J. G. and Sullivan, P. E., "Airfoil Performance at Low Reynolds Numbers in the Presence of Periodic Disturbances", *Journal of Fluids Engineering*, Vol. 128, 2006, pp. 587 - 595.

25. Yarusevych, S., Sullivan, P. E. and Kawall, J. G., "Effect of Acoustic Excitation Amplitude on Airfoil Boundary Layer and Wake Development", *AIAA Journal*, Vol. 45, No. 4, 2007, pp. 760 - 771.

26. Greenblatt, D. and Wygnanski, I. J., "The Control of Flow Separation by Periodic Excitation ", *Progress in Aerospace Sciences*, Vol. 36, 2000, pp. 487 - 545.

List of Figures

wing with acoustic excitation; c) Φ increasing without acoustic excitation; d) Φ increasing with acoustic excitation; e) Φ decreasing without acoustic excitation; f) Φ decreasing with acoustic excitation. (Note that for clarity the wing has been stretched by a factor of 2 in spanwise direction).

Figure 11. a) Velocity magnitude over flat plate wing without acoustic excitation; b) velocity magnitude with acoustic excitation; c) velocity standard deviation without acoustic excitation; d) velocity standard deviation with acoustic excitation; e) vorticity without acoustic excitation and f) vorticity with acoustic excitation. Φ = 0° and increasing, y/(b/2) = -0.5 (on left half of the wing), α = 17°, and *St* = 1.5.

Figure 12. Vorticity in a cross-flow plane near the trailing edge (x/c = -0.97) of the flat plate wing for a) stationary wing; b) Φ decreasing without acoustic excitation and c) Φ decreasing with acoustic excitation at *St* = 1.5. α = 17° and Φ = 0°.

Figure 13. Standard deviation of crossflow velocity near the trailing edge (x/c = -0.97) of the flat plate wing for a) stationary wing; b) Φ increasing without acoustic excitation and c) Φ increasing with acoustic excitation at *St* = 1.5. α = 17° and Φ = 0°.

Figure 14. High-frame-rate PIV measurements of velocity magnitude, streamlines and velocity power spectrum over the stationary flat plate wing at spanwise locations of y/(b/2) = 0 (mid-span) and α = 17°, Φ = 0°. Velocity power spectrum is calculated near the shear layer at streamwise location of x/c=0.25 for (a) without acoustic excitation, (b) with acoustic excitation at *St* = 0.6, (c) *St* = 1.5, and (d) *St* = 2.

Figure 15. High-frame-rate PIV measurements of velocity magnitude, streamlines and velocity power spectrum over the stationary flat plate wing at spanwise locations of y/(b/2) = 0.5 (right half of the wing) and α = 17°, Φ = 0°. Velocity power spectrum is calculated near

the shear layer at streamwise location of x/c=0.25 for (a) without acoustic excitation, (b) with acoustic excitation at St = 0.6, (c) St = 1.5, and (d) St = 2.

Figure 16. High-frame-rate PIV measurements of streamlines and velocity power spectrum over the stationary NACA0012 wing at spanwise locations of y/(b/2) = 0 (mid-span) and α = 17°, Φ = 0°. Velocity power spectrum is calculated near the shear layer at streamwise location of x/c=0.25 for (a) without acoustic excitation, (b) with acoustic excitation at St = 0.6, (c) St = 1.5, and (d) St = 2.

Figure 17. High-frame-rate PIV measurements of streamlines and velocity power spectrum over the stationary SD7003-085-88 wing at spanwise locations of y/(b/2) = 0 (mid-span) and α = 17°, Φ = 0°. Velocity power spectrum is calculated near the shear layer at streamwise location of x/c=0.25 for (a) without acoustic excitation, (b) with acoustic excitation at St = 0.6, (c) St = 1.45, and (d) St = 2.

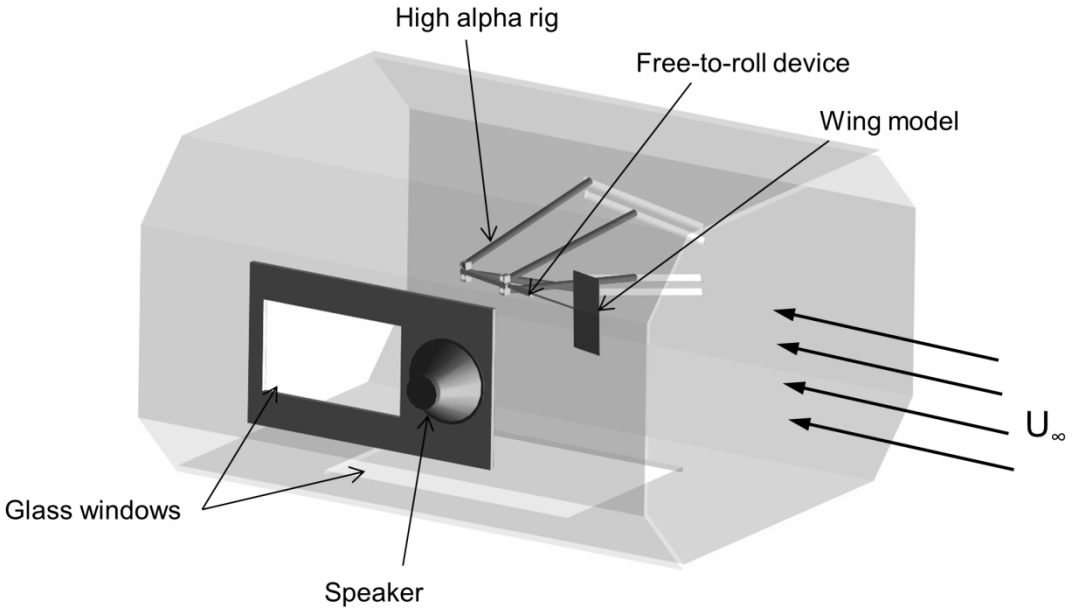

Figure 1. Schematic of the experimental setup.

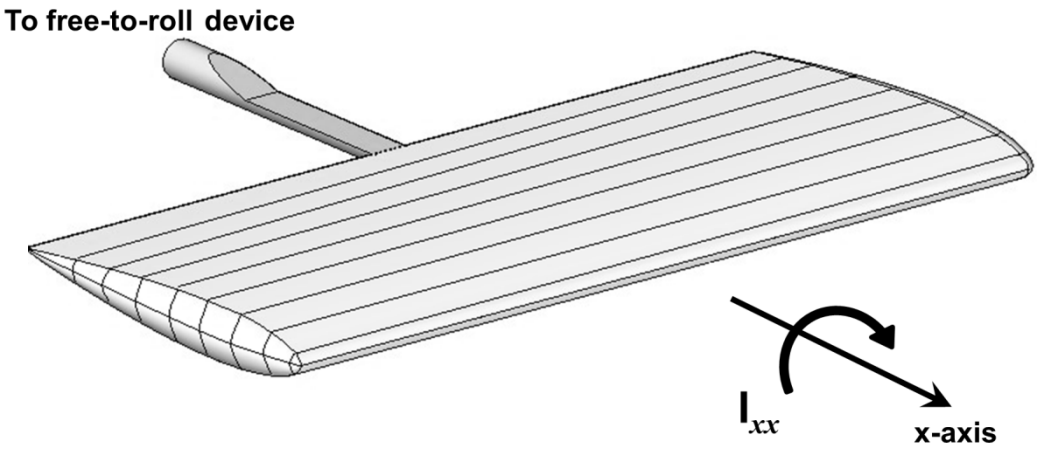

Figure 2. NACA0012 low aspect ratio wing mounted on the shaft attached to the free-to-roll device.

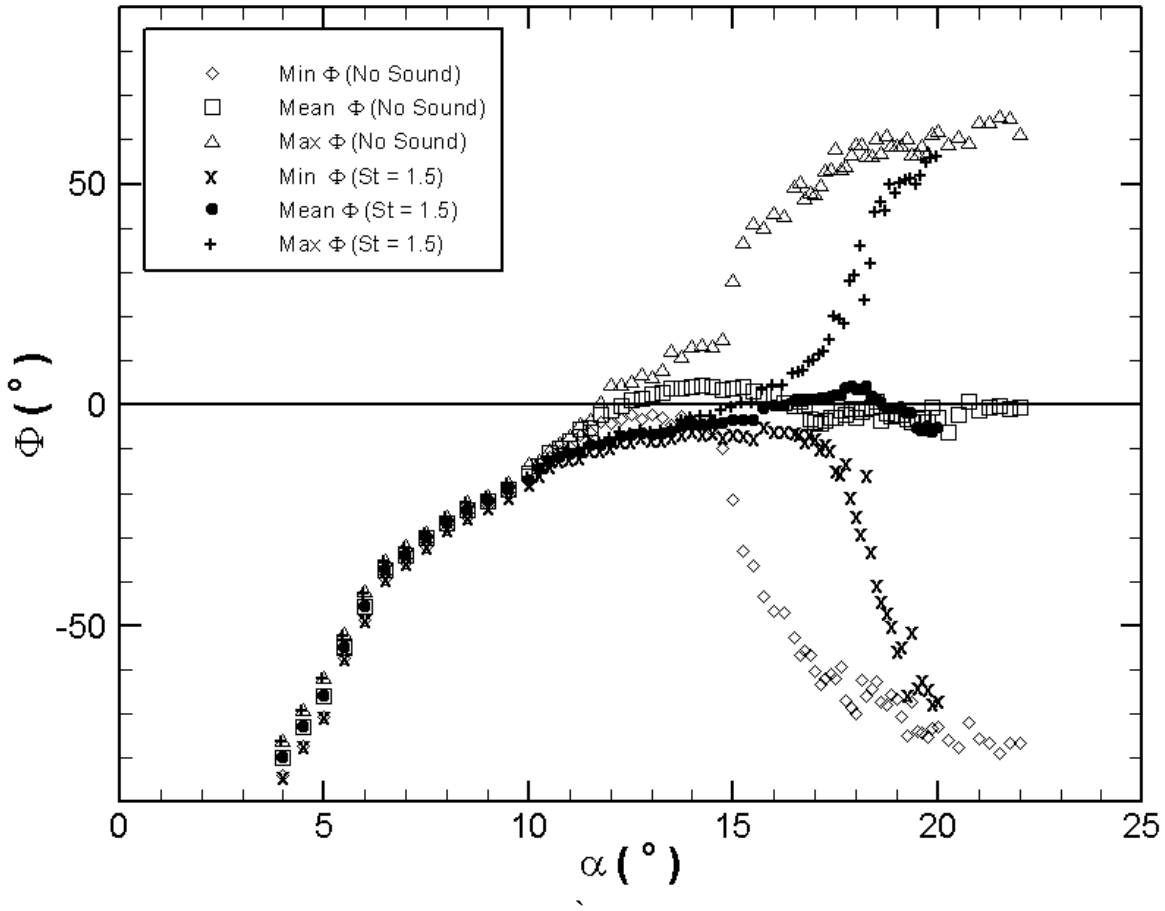

Figure 3. Variation of roll angle with angle of attack for the flat plate wing with *AR* = 2, without and with acoustic excitation at *St* = 1.5.

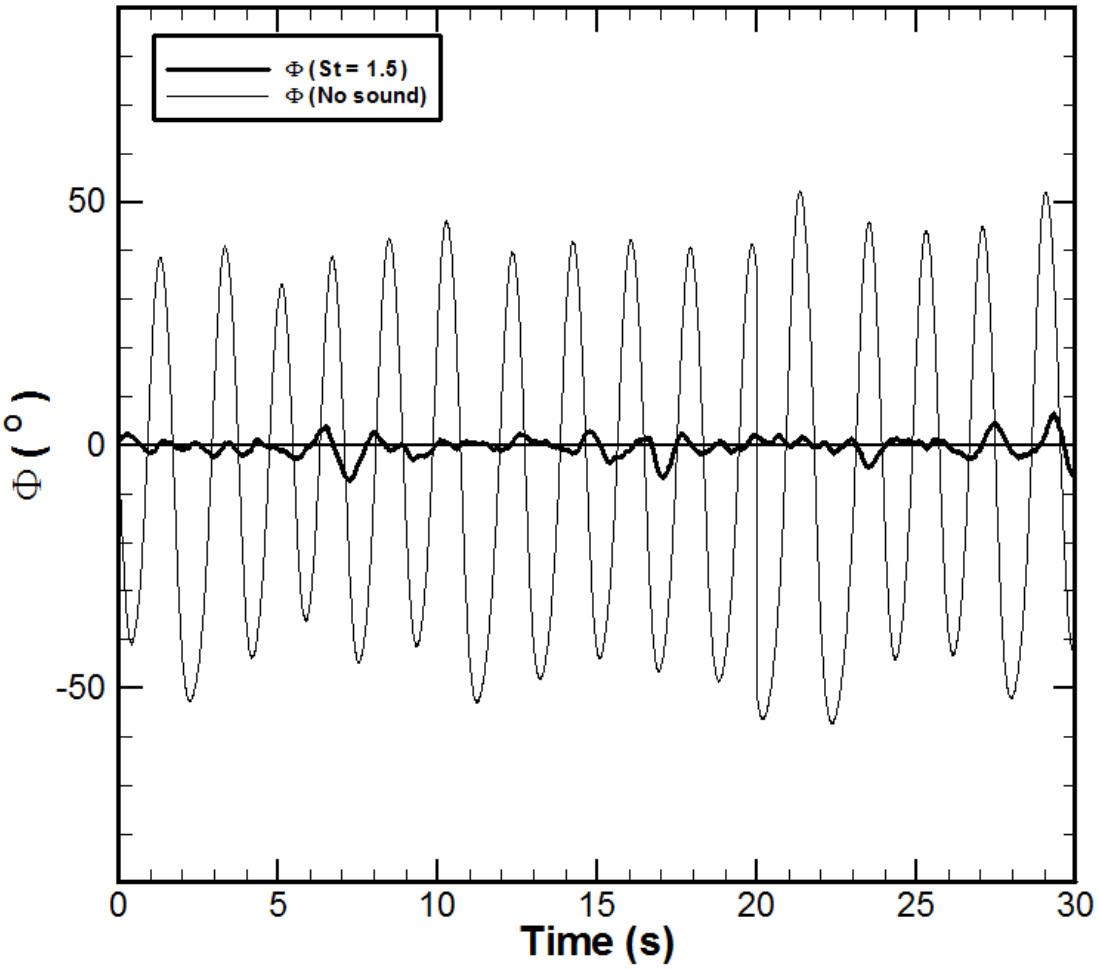

Figure 4. Time histories of the flat plate wing roll angle, without and with acoustic excitation at *St* = 1.5, α = 17°.

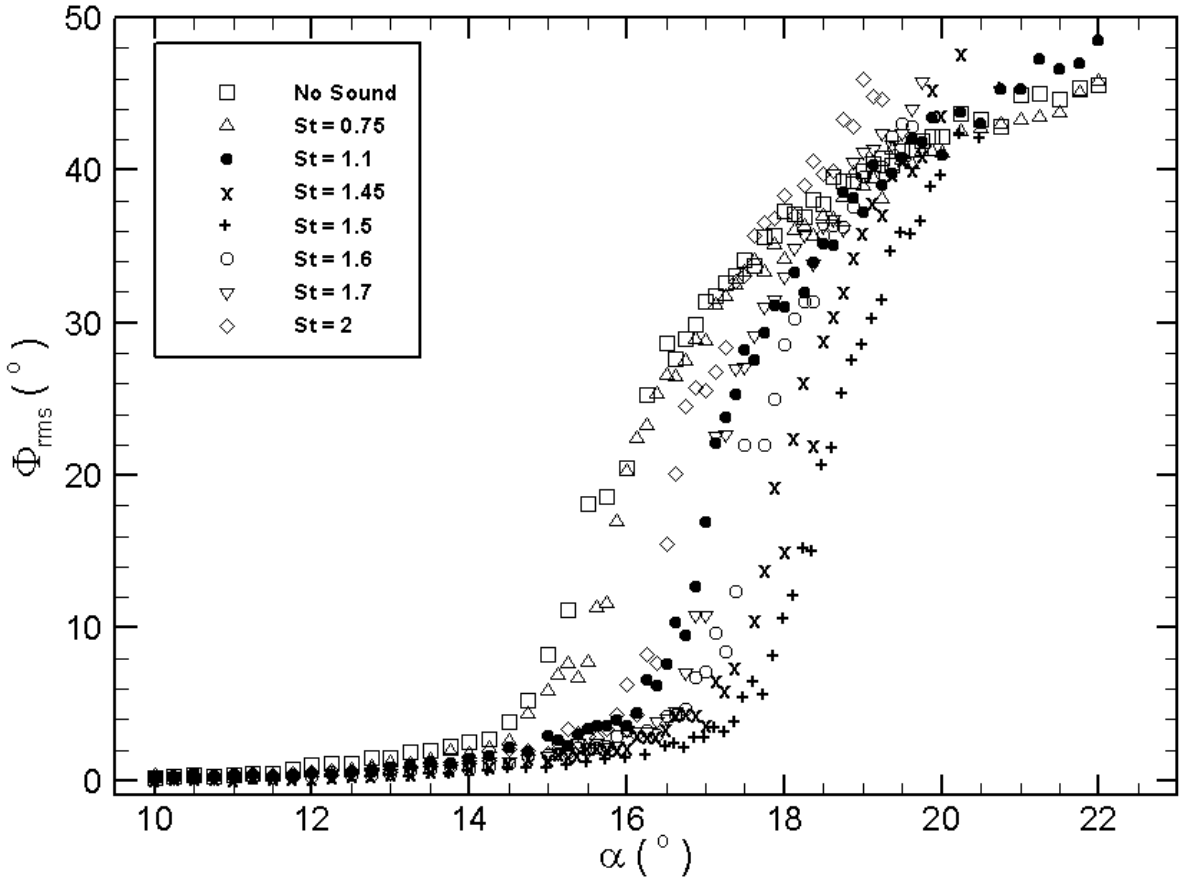

Figure 5. RMS values of the free-to-roll flat plate roll angle as a function of angle of attack without and with acoustic excitation in the range: *St* = 0.6 – 2.0.

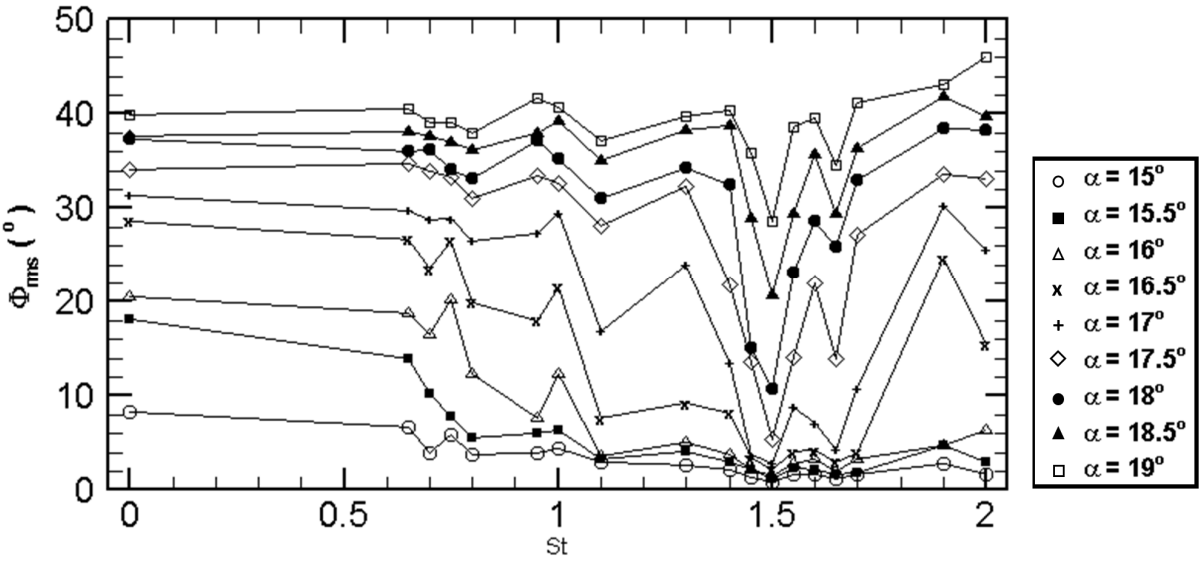

Figure 6. RMS values of the free-to-roll flat plate roll angle as a function of Strouhal number of the acoustic excitation.

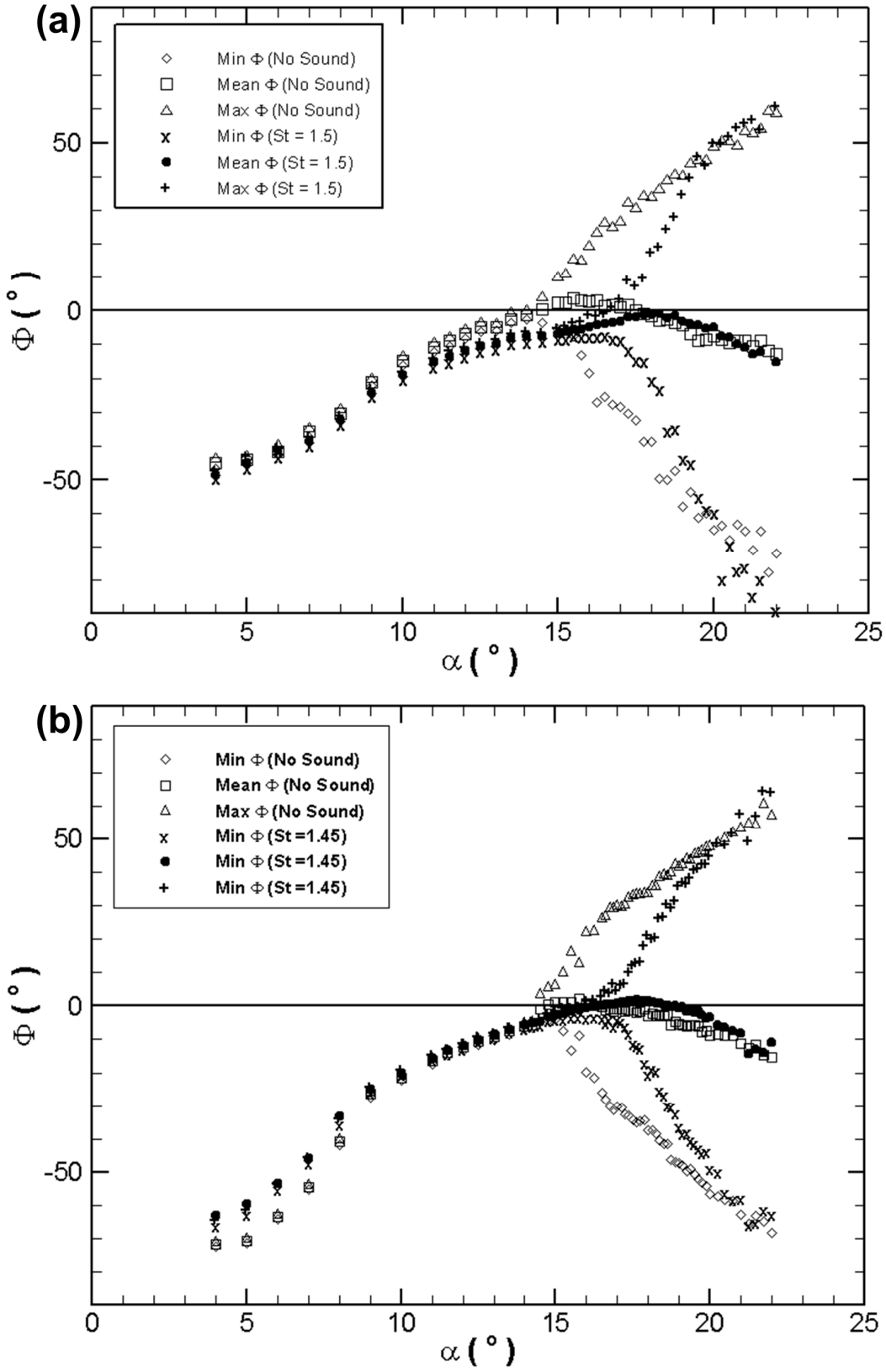

Figure 7. Variation of roll angle with angle of attack for (a) NACA0012 wing without and with acoustic excitation at *St* = 1.5, and (b) SD7003-085-88 wing without and with acoustic excitation at *St* = 1.45.

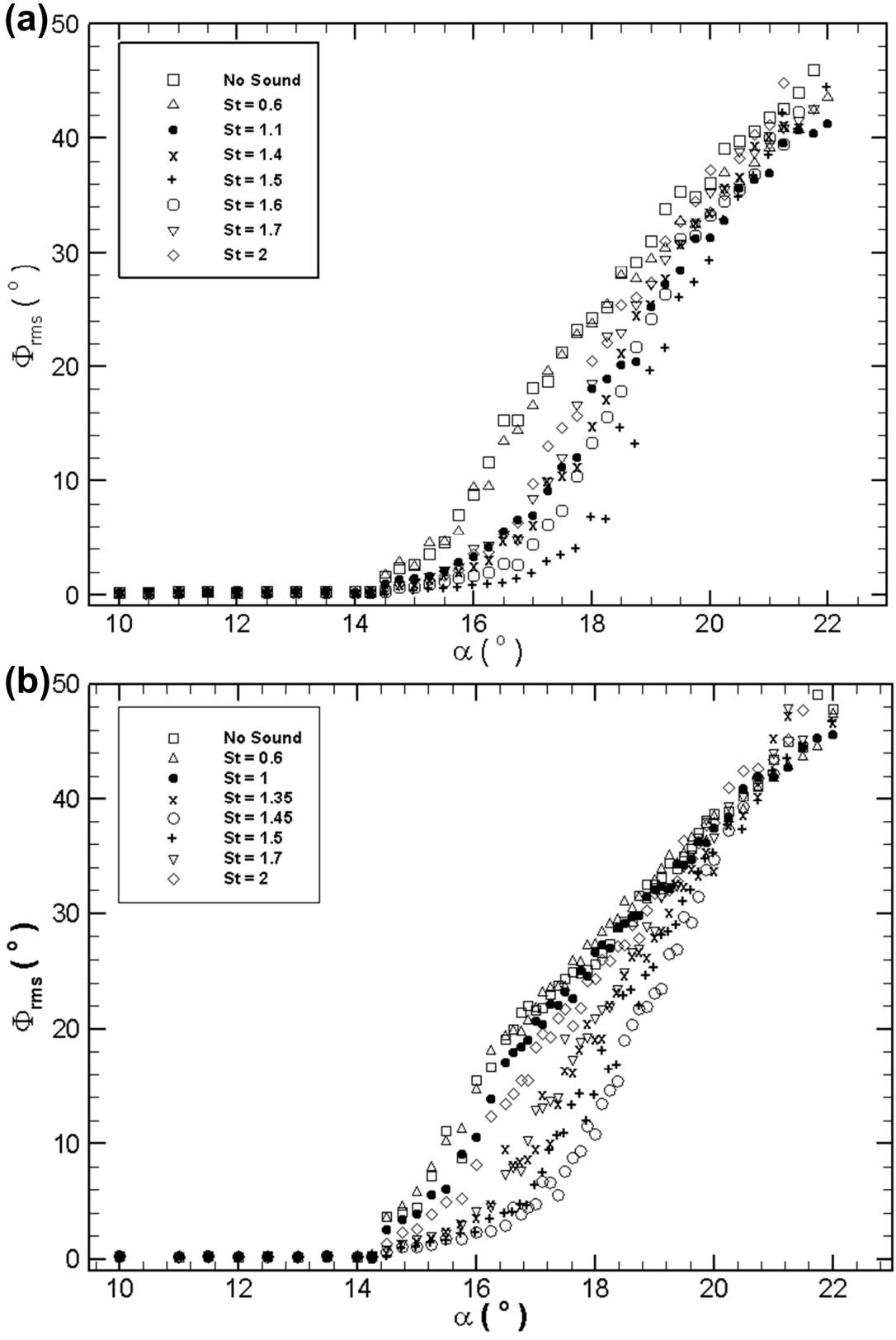

Figure 8. RMS values of the free-to-roll (a) NACA0012 wing and (b) SD7003-085-88 wing roll angles as a function of angle of attack without and with acoustic excitation in the range: *St* = 0.6 – 2.0.

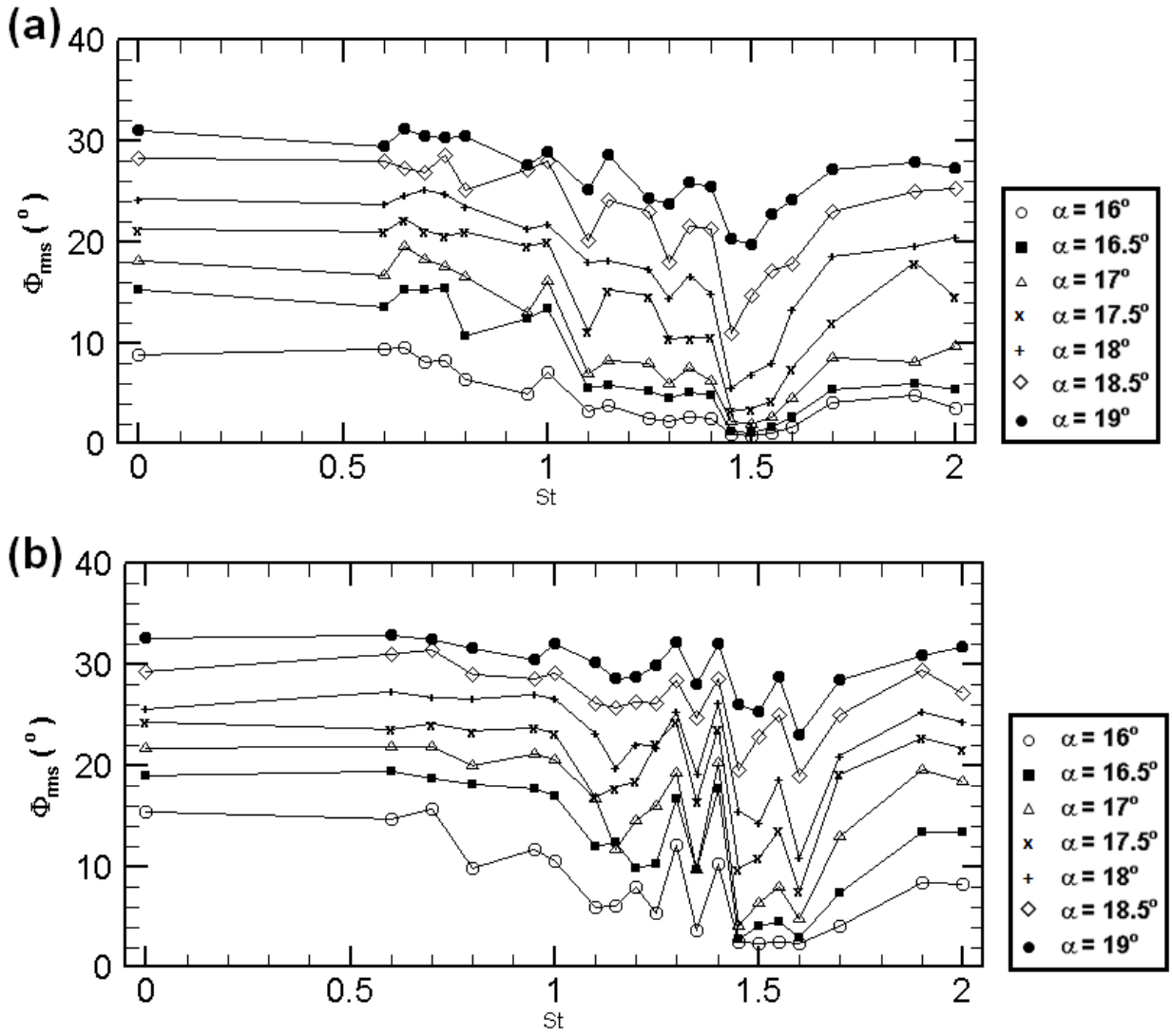

Figure 9. RMS values of the free-to-roll (a) NACA0012 wing and (b) SD7003-085-88 wing roll angles as a function of Strouhal number of the acoustic excitation.

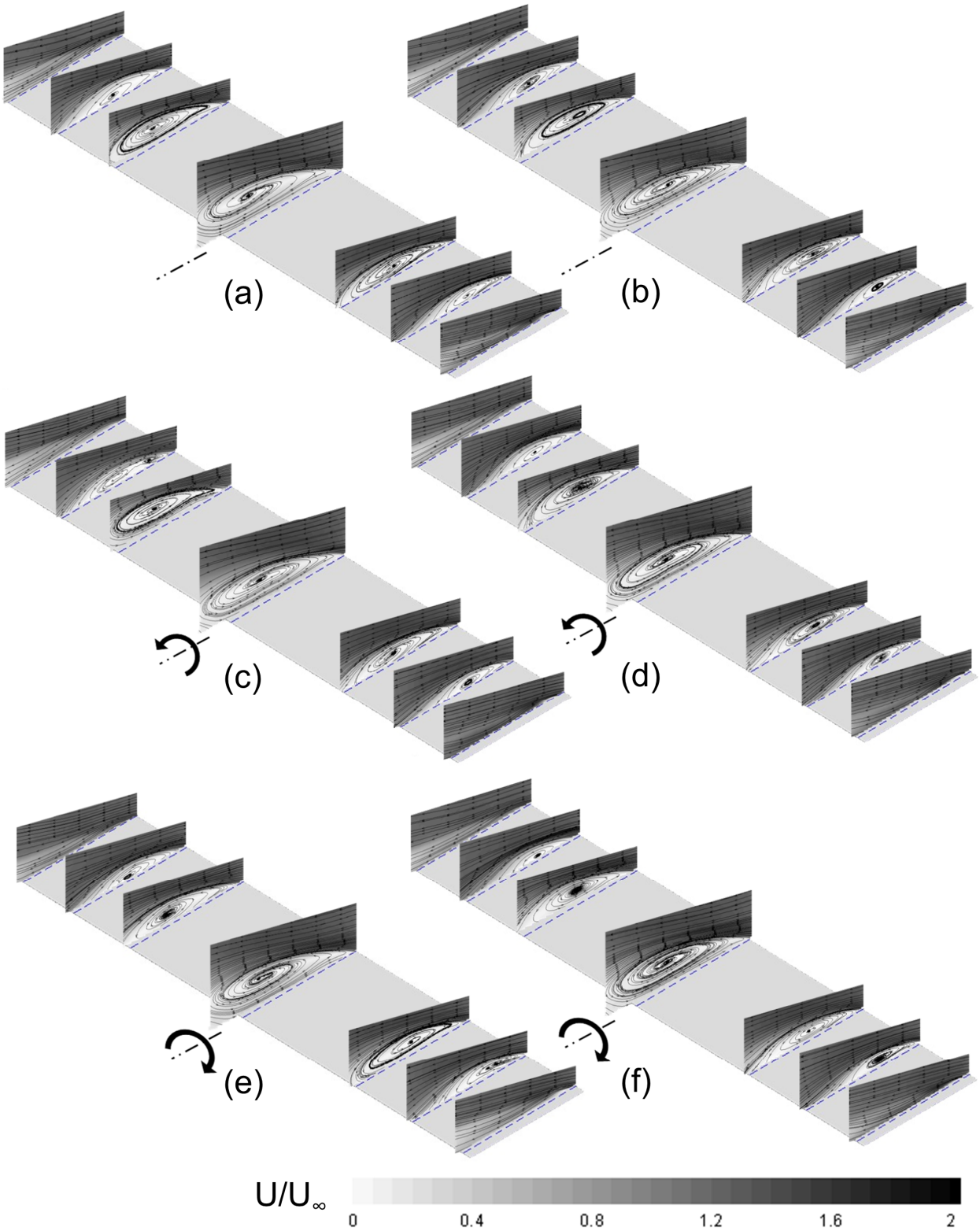

Figure 10. Velocity magnitude and streamlines over the flat plate wing at various spanwise locations of y/(b/2) = 0 (mid-span), ±0.5, ±0.75, ±0.97 and α = 17°, Φ = 0° without and with acoustic excitation at *St* = 1.5; a) stationary wing without acoustic excitation; b) stationary wing with acoustic excitation; c) Φ increasing without acoustic excitation; d) Φ increasing with acoustic excitation; e) Φ decreasing without acoustic excitation; f) Φ decreasing with acoustic excitation. (Note that for clarity the wing has been stretched by a factor of 2 in spanwise direction).

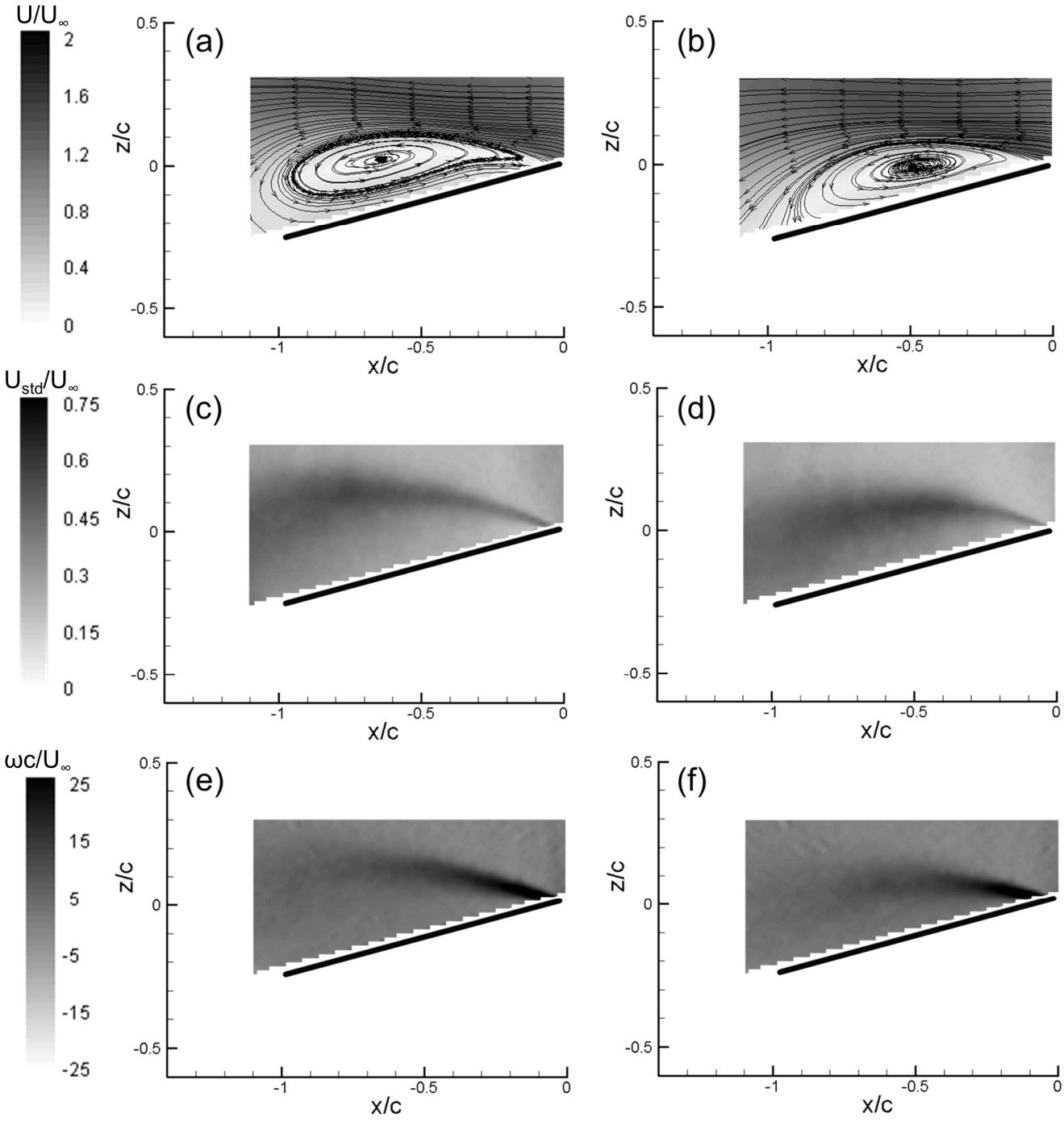

Figure 11. a) Velocity magnitude over flat plate wing without acoustic excitation; b) velocity magnitude with acoustic excitation; c) velocity standard deviation without acoustic excitation; d) velocity standard deviation with acoustic excitation; e) vorticity without acoustic excitation and f) vorticity with acoustic excitation. Φ = 0° and increasing, y/(b/2) = -0.5 (on left half of the wing), α = 17°, and *St* = 1.5.

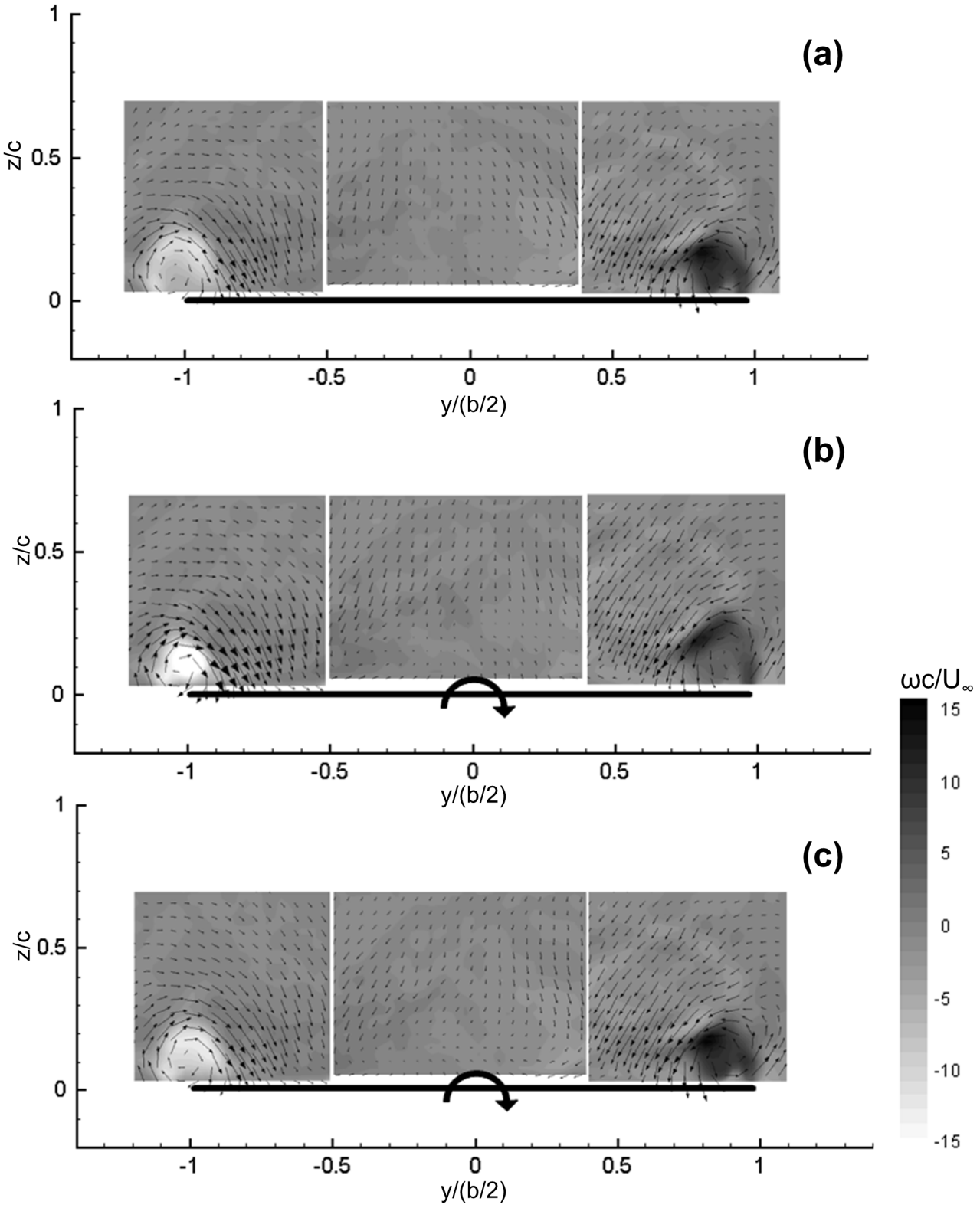

Figure 12. Vorticity in a cross-flow plane near the trailing edge (x/c = -0.97) of the flat plate wing for a) stationary wing; b) Φ decreasing without acoustic excitation and c) Φ decreasing with acoustic excitation at *St* = 1.5. α = 17° and Φ = 0°.

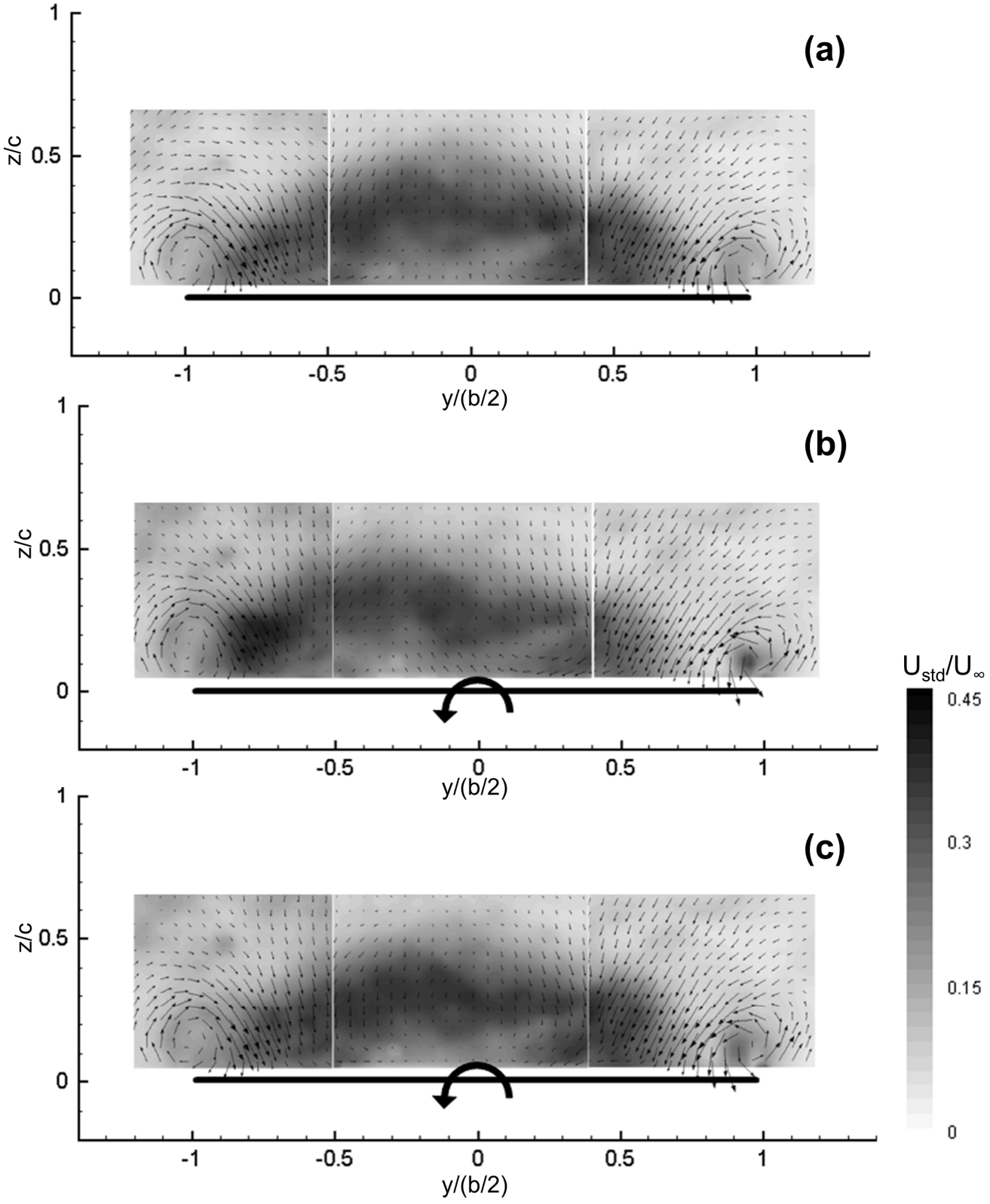

Figure 13. Standard deviation of crossflow velocity near the trailing edge (x/c = -0.97) of the flat plate wing for a) stationary wing; b) Φ increasing without acoustic excitation and c) Φ increasing with acoustic excitation at *St* = 1.5. α = 17° and Φ = 0°.

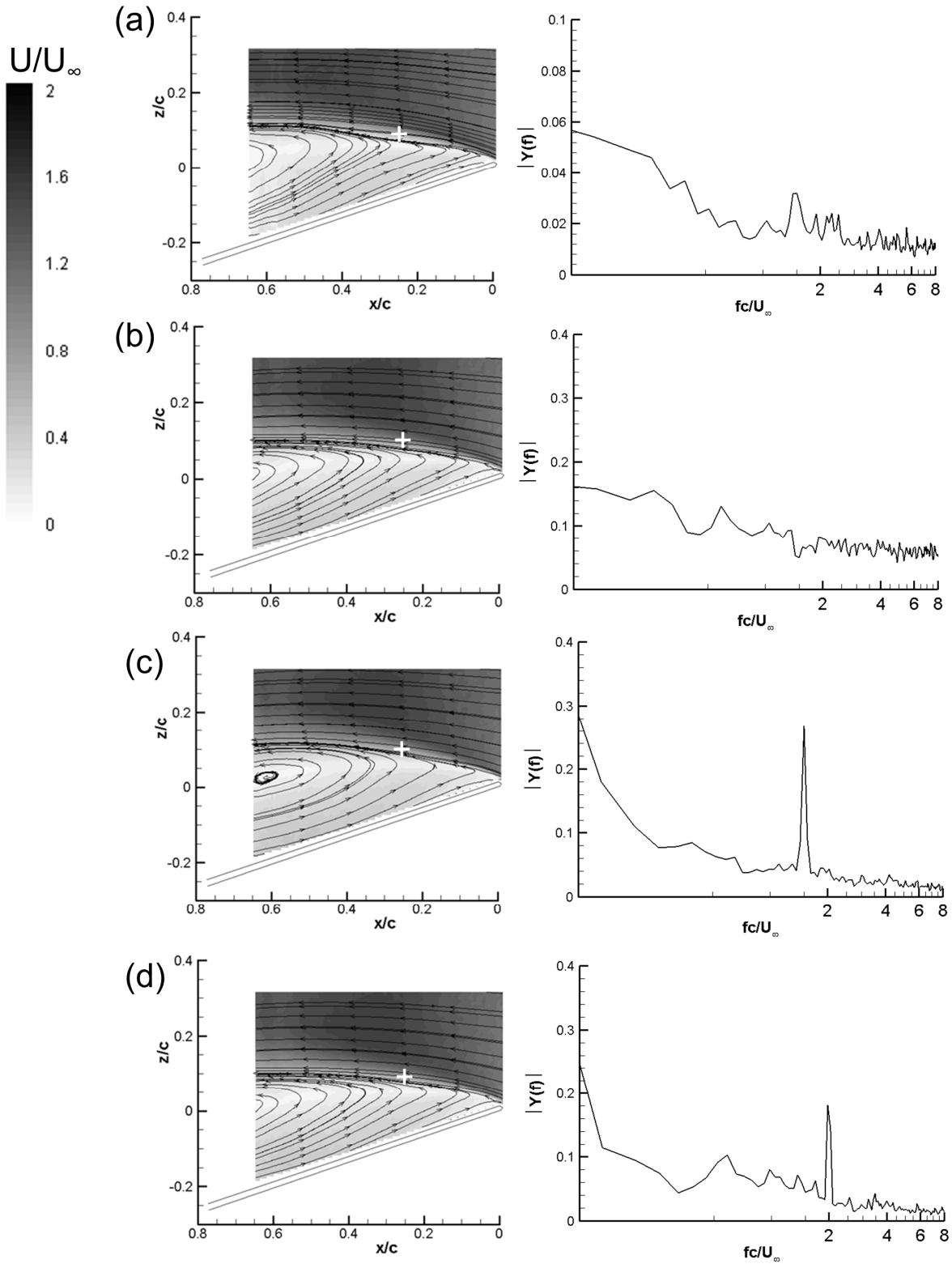

Figure 14. High-frame-rate PIV measurements of velocity magnitude, streamlines and velocity power spectrum over the stationary flat plate wing at spanwise locations of y/(b/2) = 0 (mid-span) and α = 17°, Φ = 0°. Velocity power spectrum is calculated near the shear layer at streamwise location of x/c=0.25 for (a) without acoustic excitation, (b) with acoustic excitation at *St* = 0.6, (c) *St* = 1.5, and (d) *St* = 2.

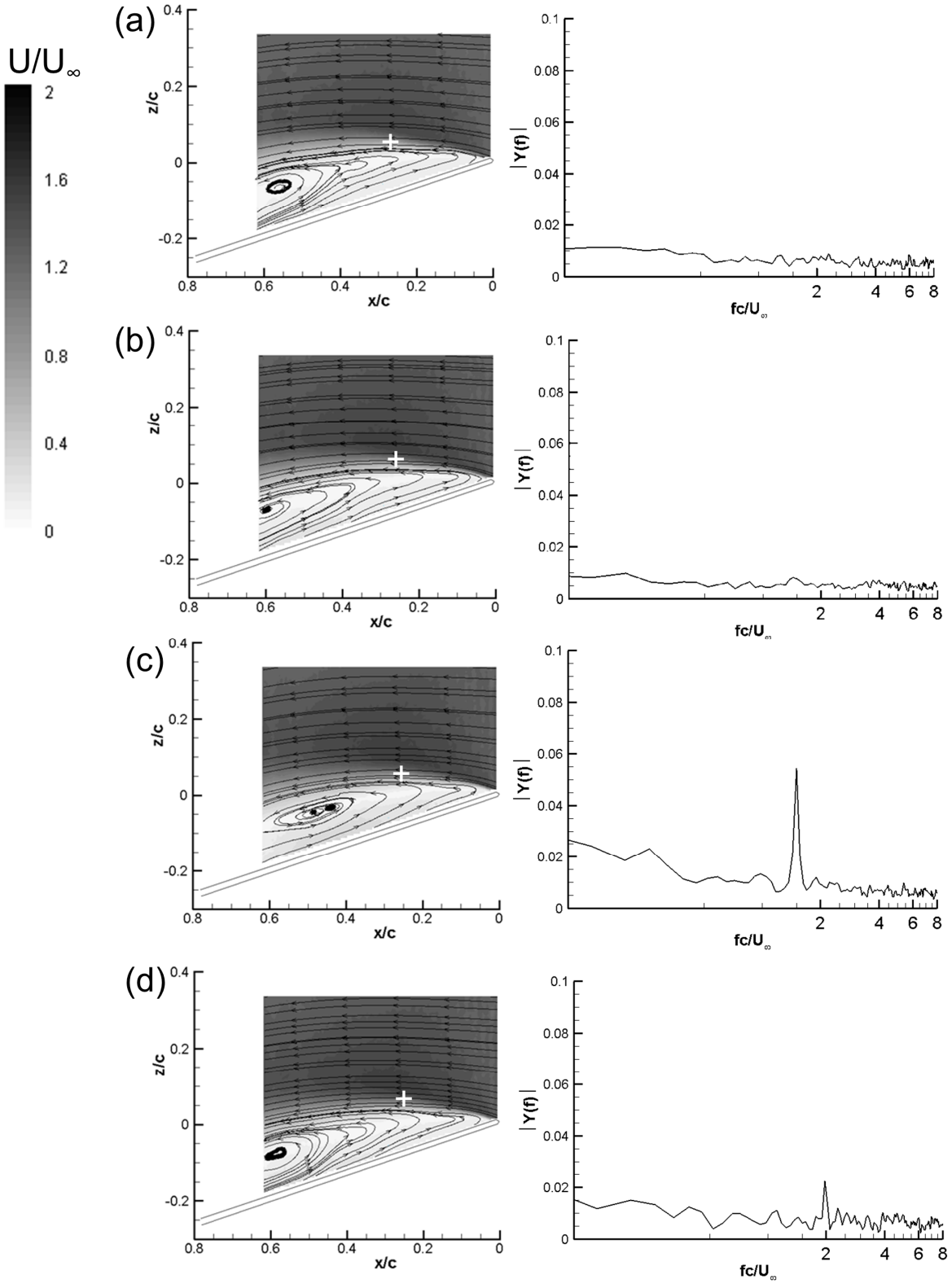

Figure 15. High-frame-rate PIV measurements of velocity magnitude, streamlines and velocity power spectrum over the stationary flat plate wing at spanwise locations of y/(b/2) = 0.5 (right half of the wing) and α = 17°, Φ = 0°. Velocity power spectrum is calculated near the shear layer at streamwise location of x/c=0.25 for (a) without acoustic excitation, (b) with acoustic excitation at *St* = 0.6, (c) *St* = 1.5, and (d) *St* = 2.

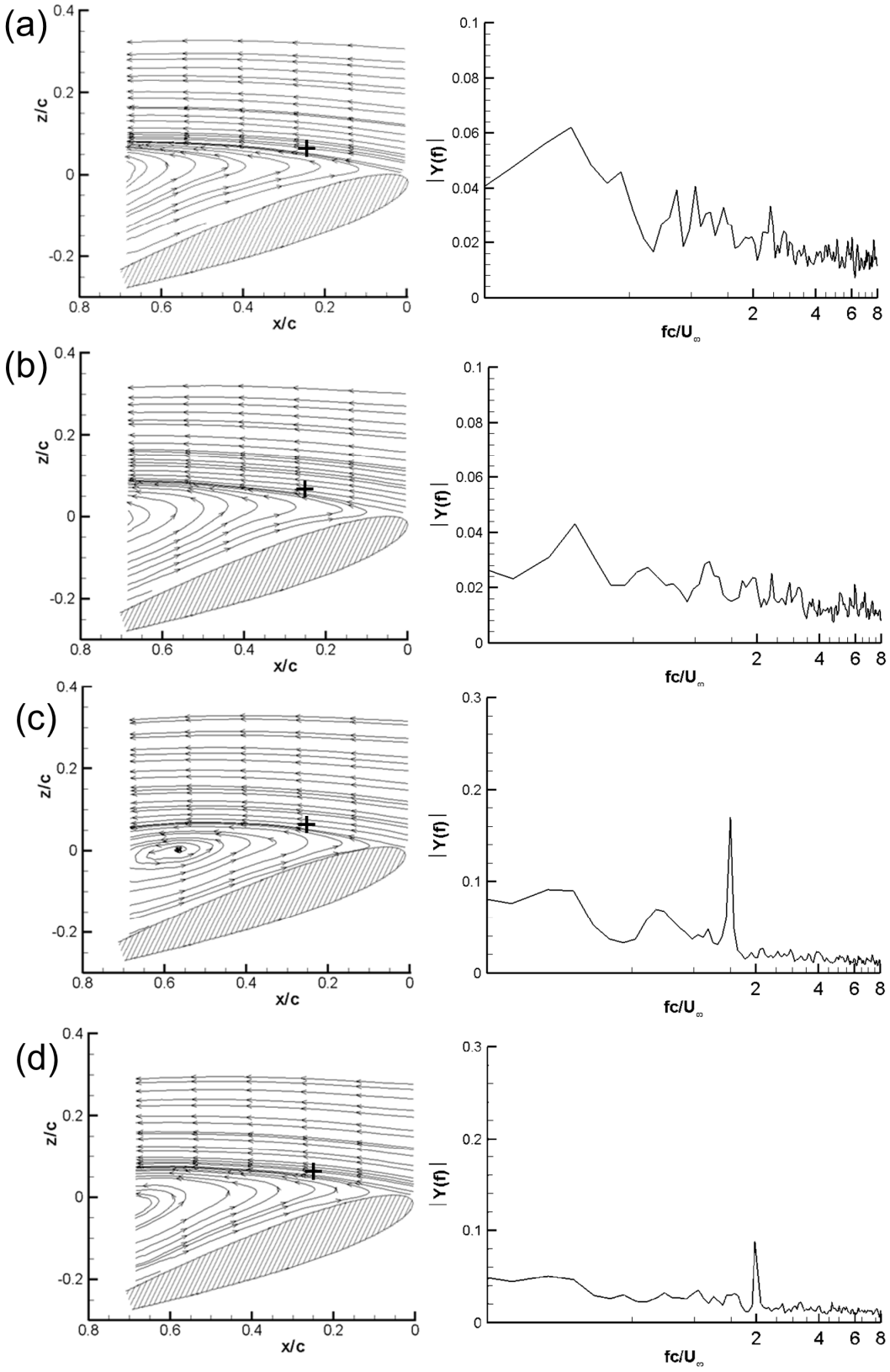

Figure 16. High-frame-rate PIV measurements of streamlines and velocity power spectrum over the stationary NACA0012 wing at spanwise locations of y/(b/2) = 0 (mid-span) and α = 17°, Φ = 0°. Velocity power spectrum is calculated near the shear layer at streamwise location of x/c=0.25 for (a) without acoustic excitation, (b) with acoustic excitation at *St* = 0.6, (c) *St* = 1.5, and (d) *St* = 2.

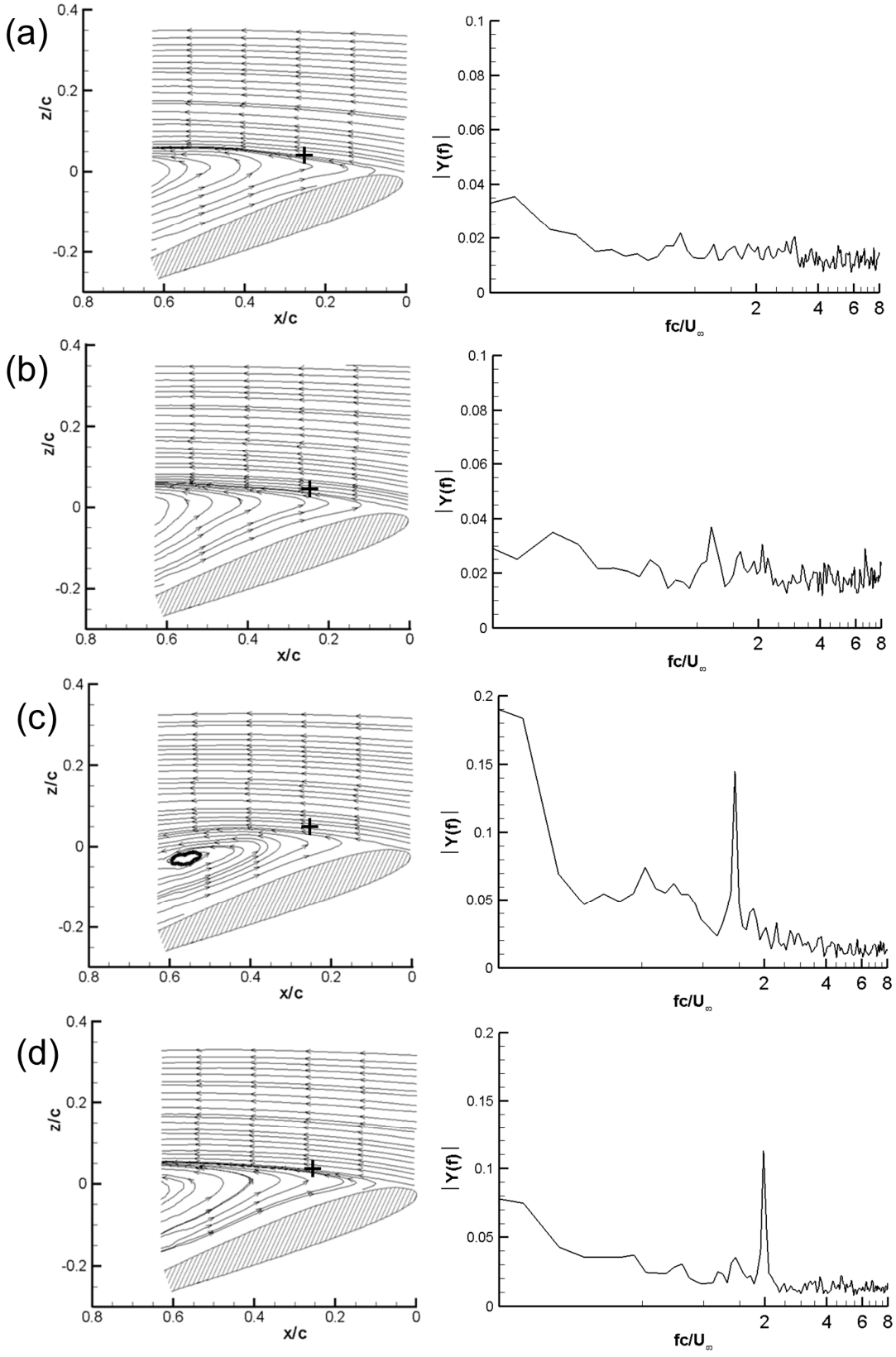

Figure 17. High-frame-rate PIV measurements of streamlines and velocity power spectrum over the stationary SD7003-085-88 wing at spanwise locations of y/(b/2) = 0 (mid-span) and α = 17°, Φ = 0°. Velocity power spectrum is calculated near the shear layer at streamwise location of x/c=0.25 for (a) without acoustic excitation, (b) with acoustic excitation at *St* = 0.6, (c) *St* = 1.45, and (d) *St* = 2.